Characterizing the Deformation Evolution with Stress and Time of Biocemented Sands

Ray Harran, S.M.ASCE[1]; Dimitrios Terzis[2]; and Lyesse Laloui, M.ASCE[3]

Abstract: Soil biocementation represents an emerging technique that has dominated the development of sustainable and innovative geotechnics during the past decade. Despite numerous studies focusing on peak strength behavior and the ensuing softening response, less is known about the stress- and time-dependent deformability of biocemented geomaterials even though it remains central for most envisaged applications. This study comprised an experimental campaign on two microbially induced carbonate precipitation (MICP)-treated sands with different initial characteristics. Samples with various calcite contents were subjected to uniaxial and incremental loading and to long-term monotonic loading to evaluate their compressibility and capture the principles of their deformation. Furthermore, the use of the porosity-to-cement ratio, originally developed for artificially bonded soils, is herein evaluated as a parameter to capture and express the behavior of MICP-treated sands. Observations from the incremental loading campaign revealed that for a range of calcite contents between 3% and 8% and for applied stress levels up to 1,000 kPa, MICP treatment significantly enhanced the stiffness properties of the geomaterials and reduced their overall deformability. Medium-grained sand required lower bond contents to achieve a similar compressibility to fine-grained sand and was more compatible with the porosity-to-cement ratio. The effects of time dependency were also assessed under different sustained monotonic loads over a long time (>75 days). Under sustained high stresses exceeding the apparent preconsolidation stress, the coefficient of secondary compression reached up to a threefold increase compared with the untreated state. Based on the behavioral characterization, stress and time considerations were shown to be interdependent. The cementation achieved by the treatment shifted a portion of immediate settlement, which was released as delayed deformation after bond breakage took place, depending on loading configuration and bond quality (deposition and imperfections), as determined via microstructural observations. **DOI: 10.1061/(ASCE)GT.1943-5606.0002871.**

Author keywords: Microbially induced carbonate precipitation (MICP); Biocementation; Soil improvement; Compressibility; Creep.

Introduction

Geotechnical solutions based on novel biomediated mechanisms and materials have gained momentum due to ever increasing awareness of the effects of traditional stabilization alternatives on the soil environment and groundwater quality. Among these solutions, microbially induced calcite (or, more generally, calcium carbonate) precipitation (MICP) emerges as the most promising biomediated improvement technique. It aims to precipitate a cementing agent underground, bonding previously unbonded or weakly bonded soil grains through biochemical processes. Urea hydrolysis is studied as the most promising precursor of calcite mineralization. More precisely, this reaction can be accelerated using urease-bearing soil microorganisms, the most common being *Sporosarcina pasteurii*. Urea hydrolysis generates carbonate ions through a series of chemical reactions summarized in Eq. (1), which then precipitates in the presence of calcium ions to form solid calcium carbonate in a supersaturated system as per Eq. (2)

$$CO(NH_2)_2 + 2H_2O \xrightarrow{\text{urease}} 2NH_4^+ + CO_3^{2-} \quad (1)$$

$$Ca^{2+} + CO_3^{2-} \rightarrow CaCO_3 \downarrow \quad (2)$$

MICP is environmentally friendly, lends itself to a wide range of natural conditions, preserves the permeability of natural terrains, and competes with traditional methods in terms of practicality, cost, and effectiveness. Most notably, this technique has been proposed to mitigate multiple underground problems by increasing the bearing capacity of soils, addressing slope stabilization problems, and achieving liquefaction mitigation (Terzis and Laloui 2019a).

Categorizing biocemented soils in an existing class of geomaterials in an attempt to better predict their response under different loading conditions remains a challenge. Depending on the geomaterial and treatment level, a clear differentiation between a soil- or rock-like product remains vague. More so, some of the most promising MICP applications, namely the biostabilization of new or existing structures, are usually not governed by ultimate strength but rather by total or differential settlement criteria. A more global understanding of the deformability of this peculiar geomaterial is thus needed. Deformability is studied through an experimental plan that aims to address (1) the stress-dependent deformability of biogeomaterials; and (2) their time-dependent deformability.

Scarce literature exists regarding the deformability of cemented soils compared with the abundance of strength-oriented literature. Additionally, most deformability studies generally target artificially cemented soils with portland cement or lime as the binding agent. For cemented soils, two key factors govern the mechanical response: packing density and cement content (Diambra et al. 2021; Xiao et al. 2020). A standard parameter linking these two factors

[1]Graduate Student Researcher, Laboratory of Soil Mechanics, Swiss Federal Institute of Technology, Lausanne 1015, Switzerland (corresponding author). Email: ray.harran@epfl.ch

[2]Postdoctoral Researcher, Laboratory of Soil Mechanics, Swiss Federal Institute of Technology, Lausanne 1015, Switzerland.

[3]Professor, Laboratory of Soil Mechanics, Swiss Federal Institute of Technology, Lausanne 1015, Switzerland.

Note. This manuscript was submitted on July 15, 2021; approved on May 12, 2022; published online on July 20, 2022. Discussion period open until December 20, 2022; separate discussions must be submitted for individual papers. This paper is part of the ***Journal of Geotechnical and Geoenvironmental Engineering***, © ASCE, ISSN 1090-0241.

was introduced for artificially cemented soils (Consoli et al. 2007) and referred to for correlations and empirical fits with mechanical performance (Consoli et al. 2012, 2013). The critical parameter used to express this density-cementation dependence is the η/C_{iv} ratio, where η is porosity and C_{iv} is volumetric content of cement. The same ratio could be applied for MICP-treated soils, similar to other approaches aiming to better identify cementation level (Nafisi and Montoya 2018). Regarding the effect of biocementation on soil compressibility, Feng and Montoya (2014) found that low cementation values, even as low as 0.2%, can have a non-negligible impact on the deformability of sands. Lee et al. (2013) proposed correlations for compression indices with varying amounts of calcite. A comparison by Lin et al. (2016) also included variations in *S*-wave velocities with increasing effective stress between different MICP treatments during confined compression tests. Few studies have accounted for the combined effects of different sand types, initial densities, and a wide range of treatment levels on deformability with incremental loading in k_0 conditions. Beyond typical geomaterials such as sand, MICP has also been proposed to mitigate the high compressibility of coal ash materials at laboratory scale (Montoya et al. 2019).

As far as time-dependent phenomena are concerned, one must first account for the various definitions and scopes found in the literature. The principal point for this work is the study of creep in its most commonly accepted definition as deformation under sustained load over time. Few studies target the creep behavior of granular soils (Mitchell and Solymar 1987; Di Prisco and Imposimato 1996). More recently, a potential origin of creep in natural sand was identified as the progressive sliding of grains at intergranular contacts (Andò et al. 2019). Beyond natural sand, most studies focusing on time-dependent characteristics usually refer to artificially cemented soils (mainly using portland cement) that are not under the influence of sustained loading. Rather, they target the time dependence in chemical dissolution contexts (Croizé et al. 2010) characterization of the effect of curing time on strength buildup. A recent study targeted the direct shear creep of MICP-treated silica and calcareous sand, suggesting an enlargement and then decline of creep deformation with treatment (Yuan et al. 2022). To the best of our knowledge, there have been no observations of creep-like behavior of MICP-treated soils in isotropic compression. Moreover, the time-dependent effects of sustained loading on the biocemented matrix remain largely unknown. As such, the complete characterization and prediction of the deformability of this material is still lacking, despite being at the core of most MICP applications as a soil improvement strategy.

In this study, both the stress- and time-dependent deformability of biocemented sands with different initial characteristics are captured. Through a series of experiments under uniaxial k_0 conditions, the deformation and variation in compressibility parameters with respect to calcium carbonate content and density are addressed in the first section, along with the adaptation of the porosity-to-cement ratio. In the following section, time dependence and its characteristics are captured with increasing and sustained loading. Both aspects are then linked in the "Discussion" section, where an interdependent stress-time behavior is proposed and elaborated.

Materials and Methods

Tested Soils

Two types of pure silica sands were used in this study: fine-grained Itterbeck sand (Smals SA, Cuijk, Netherlands) and medium-grained sand (Bernasconi, Bern, Switzerland). Both have been reported in the literature as the base geomaterials of previous MICP studies (Esnault-Filet et al. 2012; Terzis and Laloui 2019b). They were characterized using sieve analysis tests according to ASTM D422 (ASTM 2007), and their respective particle size distribution curves are shown in Fig. 1. Per the Unified Soil Classification System (USCS), both sands are labeled poorly graded SP according to ASTM D2487 (ASTM 2018). A summary of their properties is presented in Table 1.

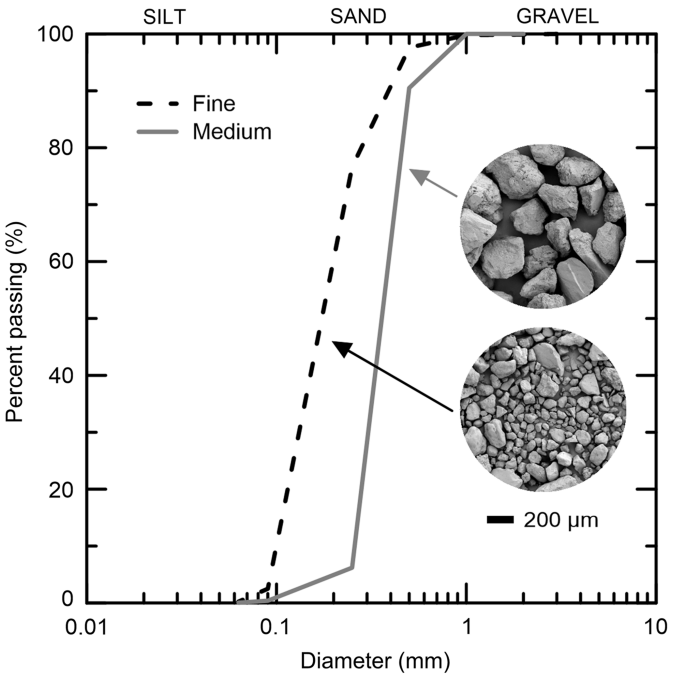

Fig. 1. Grain size distribution of tested geomaterials.

Treatment Solutions

MICP treatment was achieved through a two-solution approach, namely a bacterial solution and a urea-calcium chloride solution, referred to as the cementation solution. The composition of the solutions and their concentrations are summarized in Table 2.

Table 1. Tested geomaterials properties

Property	Medium Bernasconi	Fine Itterbeck
D_{50} (μm)	363	185
D_{10} (μm)	258	100
Minimum void ratio	0.68	0.54
Maximum void ratio	0.90	0.72
Coefficient of curvature	0.92	0.87
Coefficient of uniformity	1.5	2.0

Table 2. MICP treatment solutions

Constituent	Bacterial solution	Cementation solution
Peptone (g/L)	5	—
Lyophilized bacteria (g/L)	3	—
Urea (mol/L)	0.3	0.5
Calcium chloride (mol/L)	—	0.5
Retention time (h)	12	6

The biological preparation process was similar to that presented in Terzis and Laloui (2019b), where *Sporosarcina pasteurii* (strain designation ATCC 11859) was used as the urease-bearing bacterium. A freeze-dried state, instead of a vegetative state, was adopted as a more representative inoculum for real applications. The previously prepared bacterial powder was brought back to room temperature (25°C) and rehydrated under aerobic conditions and constant stirring in a nutrient-rich solution consisting of urea and peptone. The bacterial solution had an optical density (OD_{600}) of 0.7 and an activity of 0.32 mM/min. Distilled water was used in the preparation of all solutions. Monitoring the increase in electric conductivity (EC) allowed us to follow the hydrolysis of the added urea per Eq. (1), with an average $\Delta EC = 2.3$ mS/cm in 2 h.

Treatment Scheme

Soil samples were prepared in plastic recipients of 60-mm diameter and 120-mm height by dry pluviation and manual tamping. MICP treatment was administered by batch injections. The volume of each injection was 140 mL, or 1.2 times the pore volume, and was circulated using a peristaltic pump (MasterFlex L/S, Model 7518-10, Bruchsal, Germany) at 5 mL/min while alternating the injection-extraction inlets. An initial inoculation solution introduced the suspended bacteria into the soil, where they were allowed to attach to the sand grains for 12 h. Cementation solution batches were followed with a 6-h retention time, with pH and conductivity measurements carried out systematically before and after each injection. Once treatment was completed, samples were flushed with distilled water at a volume equal to approximately 10 times the initial pore space and then oven-dried.

Calcium Carbonate Content

The degree of cementation was determined by gravimetric acid washing. After testing, samples were oven-dried and weighed, washed with 1-M hydrochloric acid (HCl), rinsed with distilled water, oven-dried, and reweighed. The calcium carbonate content percentage (C) was then expressed as the ratio of mass change to the mass of pure soil after digestion.

The volume of calcite (V_c) following treatment, prior to any loading, can be computed from the mass of calcite (m_c) and by assuming a calcium carbonate density (ρ_c) of 2.71 g/cm^3 (smallest value within the proposed range for $CaCO_3$ between 2.7 and 2.95 g/cm^3 considering the lighter aspects of biogenic compared with geologic calcite, as later covered in the discussion section). The mass of calcite m_c is given as per Eq. (3), where m_d is the total dry mass of the sample and C is the gravimetric content. As such, V_c is obtained as per Eq. (4). The volumetric content percentage (C_{iv}) can then be expressed as the ratio of calcite volume to sample volume, while the porosity-to-cement ratio is expressed using the initial porosity before initial loading

$$m_c = \frac{C \times m_d}{1 + C} \tag{3}$$

$$V_c = \frac{C \times m_d}{\rho_c(1 + C)} \tag{4}$$

Testing Plan

Incremental Loading Series

In total, eight samples of medium-grained sand and nine samples of fine-grained sand were tested under one-dimensional compression using oedometer cells. The samples exhibited different initial dry densities and bond contents, and they were compared with untreated sand samples with similar initial densities. The dimensions of the tested samples were 60 mm in diameter and 15 mm in height. The samples were subjected to a total of eight incrementally increasing loading steps, including one unloading step in the following order: 15, 60, 125, 250, 500, 60, 500, and 1,000 kPa. Each step lasted approximately 24 per ASTM D2435 (ASTM 2020), with stabilization analysis (10-μm/12-h threshold) performed using LVDTs with an accuracy of 1 μm. A constant water level above the sample height was maintained throughout the tests.

Sustained Loading Series

Monotonic loads were sustained in the second part of the campaign presented here and were also conducted under oedometric conditions but with a different setup using the medium-grained sand previously presented. Samples were cored to the required dimensions of 50 mm in diameter and 20 mm in height. The behavior of a total of 10 samples were subjected to either a low (40 kPa) or high (400 kPa) sustained axial stress and compared with the behavior of the untreated case loaded at 400 kPa since the creep of natural sand is very small and barely perceptible at low stresses (40 kPa). The duration of the sustained loading varied 75 to 95 days between samples, with readings obtained on a frequency conforming to ASTM D2435 (ASTM 2020) over the first 24 h and 1 per day afterwards. A water level above the sample height was also maintained throughout the tests.

A summary of the samples and their respective testing conditions is given in Table 3. Samples are presented with respect to the testing series, namely incremental loading series (ILS) and sustained loading series (SLS), and sand type, namely fine-grained (F) or medium-grained (M), followed by their determined gravimetric calcium carbonate content value (ranging 2%–8%). Where it applies, the last number corresponds to the replicant order. In addition, for the SLS series the stress level is also indicated (40 or 400 kPa).

Scanning Electron Microscopy

Representative samples of medium-grained treated sand were collected before and after testing and saved for microscopy imaging. Prior to the observations, samples were coated with a 25-nm gold layer using a Quorum (Marly, Switzerland) multicoater to avoid charging effects. The samples were then observed for textural and surface characteristics of bonds and grains using a Zeiss (Oberkochen, Germany) GeminiSEM 300 scanning electron microscopy (SEM) system.

Stress Dependence Results

One-Dimensional Compression

The void ratio and axial strain versus vertical effective stress are shown in Figs. 2 and 3. The results suggest that both sands in their untreated condition yield a similar response, with slight variations, due to their varying initial characteristics. Similar findings on the comparison of these same materials in the untreated state were reported in Terzis and Laloui (2019b). At similar densities, MICP treatment enhanced the overall deformability response by reducing the accumulated strains with increasing stress level. For instance, for medium-grained sand at a similar testing void ratio ($e_0 = 0.74$), ε_a at 1,000 kPa was reduced from 2.5% for ILS-M-0-2 (untreated) to 1% and 1.5% for ILS-M-4 and ILS-M-5 (calcium carbonate contents of 4% and 5%), respectively, despite having larger e_i values (initial looser state). Similarly, for fine sand, a 4% calcium carbonate content (ILS-F-4) reduced ε_a from 2.1% for the untreated sand (ILS-F-0-1) to 1.6% (both at $e_0 = 0.56$). This improvement could

Table 3. Experimental series summary

Test No.	Sand type	Gravimetric $CaCO_3$, C (%)	Void ratio, e_i, before treatment	Void ratio, e_0 after treatment	Relative density, D_r (%)	η/C_{iv} ratio	No. of load steps	Maximum sustained load (kPa)	Duration of each load step (d)
Incremental loading series									
ILS-M-0-1	Medium	0	0.70	0.70	90	N/A	8	1,000	1
ILS-M-0-2	Medium	0	0.74	0.74	75	N/A	8	1,000	1
ILS-M-3-1	Medium	3	0.74	0.70	71	23.6	8	1,000	1
ILS-M-3-2	Medium	3	0.75	0.70	68	23.1	8	1,000	1
ILS-M-3-3	Medium	3	0.76	0.71	62	23.4	8	1,000	1
ILS-M-3-4	Medium	3	0.78	0.73	53	24.1	8	1,000	1
ILS-M-4	Medium	4	0.79	0.73	49	21.0	8	1,000	1
ILS-M-5	Medium	5	0.83	0.74	33	15.6	8	1,000	1
ILS-F-0-1	Fine	0	0.56	0.56	90	N/A	8	1,000	1
ILS-F-0-2	Fine	0	0.59	0.59	75	N/A	8	1,000	1
ILS-F-4	Fine	4	0.63	0.56	50	13.1	8	1,000	1
ILS-F-5	Fine	5	0.61	0.53	62	10.8	8	1,000	1
ILS-F-6-1	Fine	6	0.54	0.46	99	8.9	8	1,000	1
ILS-F-6-2	Fine	6	0.62	0.54	54	10.0	8	1,000	1
ILS-F-7-1	Fine	7	0.58	0.48	80	7.4	8	1,000	1
ILS-F-7-2	Fine	7	0.55	0.45	92	6.5	8	1,000	1
ILS-F-8	Fine	8	0.64	0.52	46	6.8	8	1,000	1
Sustained loading series									
SLS-2-40	Medium	2	0.76	0.72	64	31.5	1	40	75
SLS-3-40	Medium	3	0.78	0.73	55	25.6	1	40	75
SLS-4-40-1	Medium	4	0.84	0.79	26	23.7	1	40	95
SLS-4-40-2	Medium	4	0.84	0.78	27	20.6	1	40	95
SLS-0-400	Medium	0	0.77	0.77	60	N/A	1	400	75
SLS-2-400-1	Medium	2	0.74	0.71	73	41.1	1	400	95
SLS-2-400-2	Medium	2	0.80	0.77	46	39.9	1	400	95
SLS-3-400-1	Medium	3	0.79	0.74	49	26.0	1	400	95
SLS-3-400-2	Medium	3	0.79	0.74	48	23.0	1	400	75
SLS-4-400	Medium	4	0.76	0.70	63	20.1	1	400	75

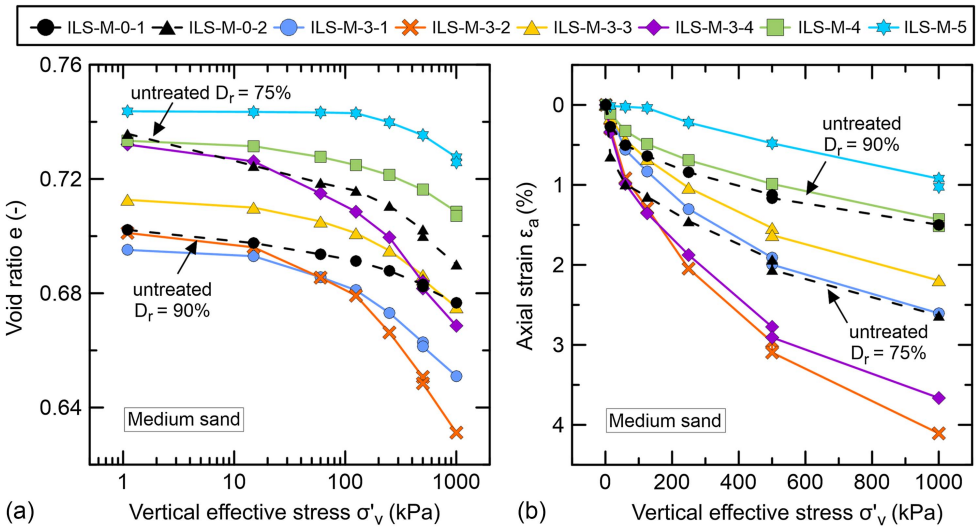

Fig. 2. Variation in (a) void ratio; and (b) axial strain with vertical effective stress for medium-grained sand.

be explained by the coupled effects of densification and bonding induced by treating the sand fabric.

At lower stresses, the predominant mechanism governing the response was bonding, as the observed enhancement improved with increasing bond content, with little to no effect of the initial void ratio of the samples. As stresses increased, the results progressively diverged, where eventually, at 1,000 kPa, the total accumulated axial strains could not be explained solely by calcium carbonate content without considering initial densities. A gradual loss of soil structure was inferred with increasing stresses, during which bonds broke while the sample accumulated more deformation until the behavior converged back to that of the uncemented state of the

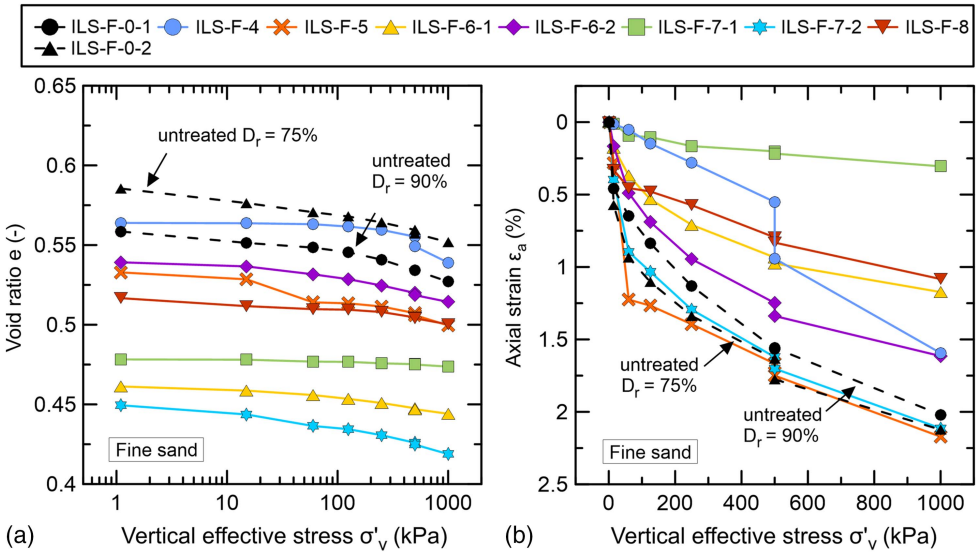

Fig. 3. Variation in (a) void ratio; and (b) axial strain with vertical effective stress for fine-grained sand.

granular assembly, predominantly governed by compacity. Note that pure calcite and silica grains exhibit different bulk moduli and similar shear moduli. More precisely, their shear moduli are comparable at approximately 44 and 32 GPa for quartz and calcite, respectively, while their bulk moduli differed by a factor of 2 at 37 and 73 GPa, respectively (Belkofsi et al. 2018; Schmitt 2015; Wang et al. 2015). However, calcite bonds resulting from MICP should not be considered pure geologic calcite due to the complex nucleation and growth processes that have been reported to yield bonds with nano- to microscale impurities and dislocations (De Yoreo et al. 2015). For the medium sand, ILS-M-0-2 (untreated) and ILS-M-3-1 (3% $CaCO_3$) converged progressively toward the same total accumulated axial strain at 1,000 kPa, while ILS-M-3-4 (3% $CaCO_3$) eventually reached a larger ε_a compared with ILS-M-0-2 since it corresponded initially to a looser state (e_i of 0.78 and 0.74, respectively). With progressive damage caused by increasing stress, the bond contribution to the overall response was gradually taken over by compacity, as both samples had the same initial void ratio before the MICP treatment, with $e_i = 0.74$. The same was observed for the fine sand, with ILS-F-0-1 (untreated) and ILS-F-7-2 (7% $CaCO_3$) having the same $e_i = 0.56$. The divergence observed between samples at the final loading step was thus dependent on the initial compactness (e_i), treatment level (% $CaCO_3$), and accumulated damage, itself a function of the treatment efficiency (number of induced active bonds) and applied stress. Overall, the results agreed with the values and trends identified in other works dealing with MICP-treated sands (Feng and Montoya 2014; Lin et al. 2016).

Most cemented samples with low or high calcium carbonate contents exhibited a continuous accumulation of deformations in their response to increasing load without immediate collapse, which has sometimes been reported in works dealing with artificially cemented soils using portland cement (Yun and Santamarina 2005) or soil cementation in general (Länsivaara 2020). The immediate collapse behavior was shown to depend primarily on the state of compactness (loose) of the base material. This was notably the case for two loose fine sand samples, ILS-F-5 ($D_r = 62\%$) and ILS-F-4 ($D_r = 50\%$), which exhibited large settlements at initial loading and at unloading-reloading at 500 kPa, respectively. Overall, the behavior of the MICP-treated and artificially cemented sands (Yun and Santamarina 2005) remained in the same range at similar compactness and (bio)cement contents.

Stress-Dependent Characteristics

The variation in ε_a with the porosity to cement ratio η/C_{iv} is shown in Fig. 4 at different stress levels. A power law ($Y = kX^{\alpha}$) was used to fit the measured strains with the η/C_{iv} ratio, as proposed in other studies (Consoli et al. 2012, 2013, 2019). For medium sand at low stresses, satisfactory relationships were established ($R^2 > 0.9$); however, these relationships were not maintained at higher stresses, where degradation of bonding led to rapid deformation and the development of compaction bands. Eventually, at the maximum stress of 1,000 kPa, the calcite bond content in the matrix, quantified either in gravimetric terms (C) or in volumetric terms (C_{iv}), was no longer a suitable parameter to capture the

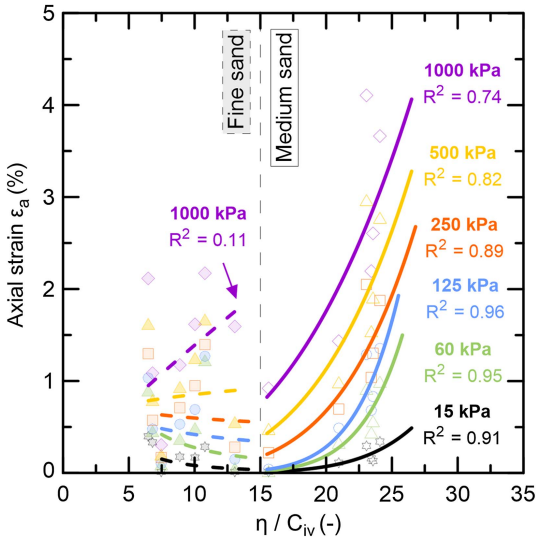

Fig. 4. Variation in accumulated axial strain with porosity-to-cement ratio at different stress levels for medium- and fine-grained sands.

mechanical response due to the irreversible loss of active bonds in the soil skeleton. This degradation front was captured when comparing successive increasing stress levels. Shear-wave velocity measurements (Montoya et al. 2019) also validated the degradation front phenomenon in similar setups and for loading-unloading cycles. Fine sand had a poor correlation with the η/C_{iv} ratio, especially considering the narrow margin of η/C_{iv} values. Note that the ratio was originally conceived for artificially cemented soils, essentially using portland cement and thus assumed the contribution of most of the cementing agent in the mechanical response. Multiple studies, however, have reported a lower efficiency for MICP treatment in fine soils (Tang et al. 2020; Terzis and Laloui 2018). As such, a high percentage of $CaCO_3$ content was recorded for fine sand, but fewer active bonds actually contributed to the stiffening of the soil. This variation in the proportion of active/passive precipitated $CaCO_3$ was also at the root of the discrepancy between replicate samples, which were extruded from different recipients yet had similar initial void ratios and treatment levels, eventually resulting in different accumulated strains upon loading. In those cases, such as for ILS-M-3-1 and ILS-M-3-2 for the medium sand and ILS-F-7-1 and ILS-F-7-2 for the fine sand, despite similar compacity and treatment levels, a divergence in the efficiency of the treatment was noted with regard to the mechanical improvement, potentially due to the formation of shear bands and inner fabric collapse.

Table 4. Incremental loading series summary coefficients

Test No.	Compression index, C_c	Recompression index, C_r	Preconsolidation stress, p_c' (kPa)
Medium sand			
ILS-M-0-1	0.019	0.005	156
ILS-M-0-2	0.033	0.004	175
ILS-M-3-1	0.033	0.002	62
ILS-M-3-2	0.056	0.003	80
ILS-M-3-3	0.033	0.003	95
ILS-M-3-4	0.043	0.005	55
ILS-M-4	0.023	0.003	156
ILS-M-5	0.023	0.002	250
Fine sand			
ILS-F-0-1	0.023	0.008	186
ILS-F-0-2	0.017	0.007	122
ILS-F-4	0.033	0.003	200
ILS-F-5	0.020	0.003	60
ILS-F-6-1	0.010	0.002	40
ILS-F-6-2	0.017	0.002	30
ILS-F-7-1	0.004	0.001	110
ILS-F-7-2	0.020	0.002	85
ILS-F-8	0.013	0.001	400

The compression index (C_c), recompression index (C_r), and preconsolidation stress (p_c') values are summarized in Table 4, as determined for the range of applied vertical stress (up to 1,000 kPa). Values of C_c typically varied between 0.010 and 0.056, falling within the established range for loose to dense quartz sands (Mesri and Vardhanabhuti 2009). MICP treatment was not observed to largely alter C_c values, as Lee et al. (2013) noted, suggesting that the $CaCO_3$ minerals lost their function under a high applied stress. The values of C_r ranged 0.004–0.007 for the natural sands and decreased to 0.001–0.003 following MICP treatment. The unloading step from 500 to 60 kPa highlighted the sensitivity of the response to loading history, where even at the previously experienced stress level of 500 kPa, additional destructuration was observed, similar to that reported in Mendoza-Ulloa et al. (2020). Values of p_c' depended on both the initial void ratio and the cementation level, with a linear decrease with increasing η/C_{iv} for medium sand ($R^2 = 0.96$) but poorer correlation for fine sand, consistent with that previously established.

The oedometric modulus (E_{oed}) for each step is shown in Fig. 5. When first comparing the untreated states, as expected, denser packing increased stiffness. For fine sand, the early compaction of the loose natural state under increasing stresses rendered its E_{oed} practically similar to the dense state. In contrast, MICP-treated samples showed an increased stiffness compared with their representative loose state before treatment. Similar findings were reported by Feng and Montoya (2016). For some cases, distinctively higher E_{oed} values were noted in at approximately 450 MPa for ILS-M-5 (5% $CaCO_3$) and 700 MPa for ILS-F-7-1 (7% $CaCO_3$) for medium- and fine-grained sands, respectively. Such values were more comparable with those of natural sandstone samples than with those of artificially cemented sands (Lashin et al. 2021; Wichtmann et al. 2017), embodying the intermediate state of biocemented geomaterials between soils and soft rock. Unlike the untreated state, little improvement was noted for treated samples with increasing stresses since the rearrangement of grains into a denser packed state was blocked by the active bonds. In contrast, notable drops in E_{oed} were eventually observed for the same samples, ILS-M-5 and ILS-F-7-1. Only the mild improvement effect due to densification was permanently retained.

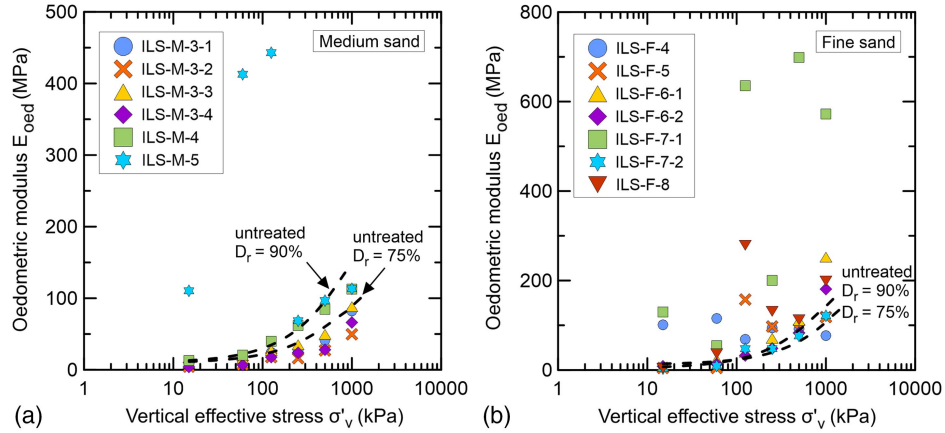

Fig. 5. Variation in oedometric modulus with vertical effective stress for (a) medium-grained; and (b) fine-grained sands.

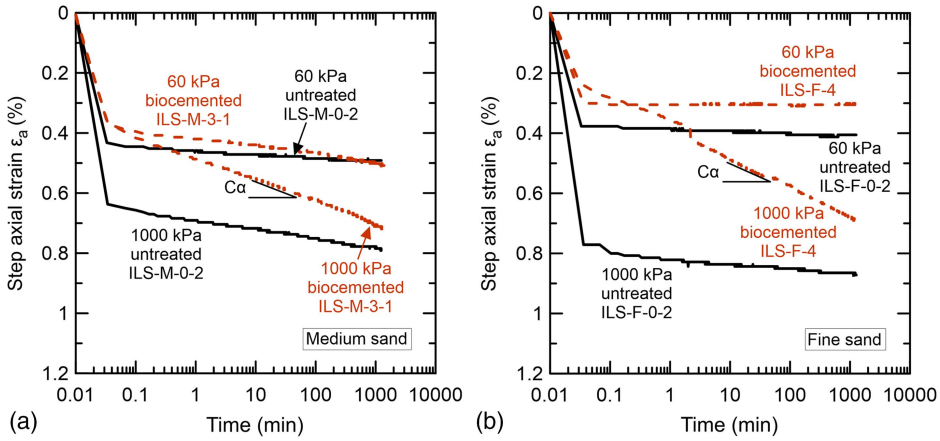

Fig. 6. Loading steps at 60 and 1,000 kPa of treated and untreated states for (a) medium-grained; and (b) fine-grained sands.

Time Dependence Results

Secondary Compression

A typical result is shown in Fig. 6, where a sample of both treated states (ILS-M-3-1 and ILS-F-4) and untreated states (ILS-M-0-2 and ILS-F-0-2) are compared at low (60 kPa) and high (1,000 kPa) stresses. For both sands, the major contributor to the total recorded settlement was immediate settlement, with more than 90% of the total ε_a attained just after the load was applied. At 60 kPa, MICP did not greatly alter overall behavior, as a large portion of ε_a was still quasi-instantaneous for the biocemented cases. It is postulated that this was the result of asperity closures, as not all grain-to-grain contacts were expected to be biocemented. However, at higher stress (1,000 kPa), the share of immediate settlement was reduced to only 45% of the step's total axial strain. Noticeably, the proportion of secondary, or delayed, deformation was higher for biocemented samples and for higher stresses.

A quantification of the secondary deformation of each loading step is provided using the coefficient of secondary compression (C_α). All values of C_α for both sands are summarized in Fig. 7. Loose natural sands had consistently higher values than the denser state at each stress level. C_α values also slightly increased with increasing stresses. In comparison, biocemented samples followed an overall similar trend, albeit with a different magnitude. Overall, at low stresses the C_α values for MICP-treated cases were similar to those of natural sands. However, as the applied stress increased, so did the C_α values, which progressively exceeded those of the untreated states. In some instances, such as for ILS-M-3-2 (medium) and ILS-F-4 (fine), C_α at 1,000 kPa exceeded the loose untreated state by a factor of 3. Since C_α decreases with increasing density and increases with increasing stress, a plateau was observed, for instance between 15 and 500 kPa, for each natural sand due to compensation between the latter effects. No similar situation was observed for the treated cases, as they did not benefit from large compaction, consistent with what was observed for E_{oed}.

Sustained Loading

The results of the sustained loading series are shown in Fig. 8. In accordance with previous results, most recorded deformation

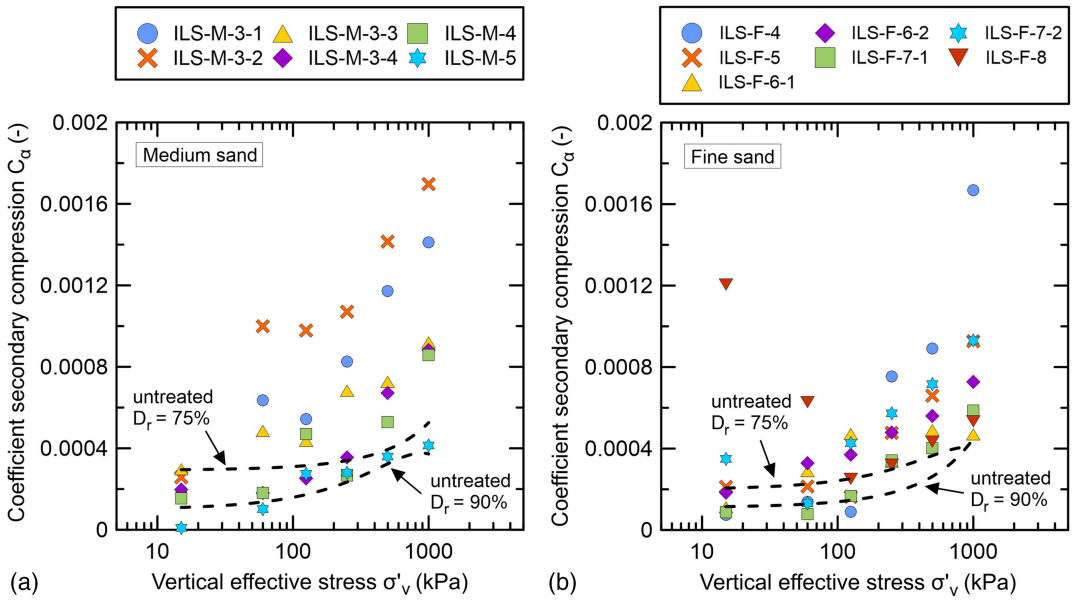

Fig. 7. Variation in the coefficient of secondary compression with vertical effective stress for (a) medium-grained; and (b) fine-grained sands.

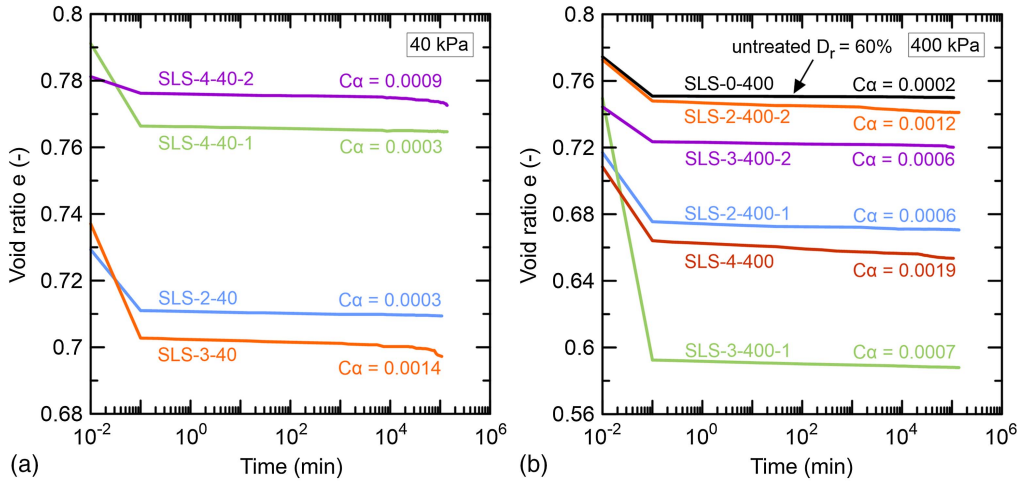

Fig. 8. Variation in void ratio under a sustained effective vertical stress of (a) 40 kPa; and (b) 400 kPa.

okto place at the end of primary consolidation in less than 5 s. Despite some additional deformation sustained over the three-month loading duration, no major collapse in void ratio was noted. For natural sand, the sustained load over 75 days yielded similar results to those for a regular incremental load step, validating the low time-dependent deformability of quartz sand, for which a quasi-negligible C_α was recorded independently of the loading duration. Most biocemented samples had C_α values within the established range, as captured via the ILS campaign. As such, the imposed stress remained the main determinant of the contribution of secondary compressibility for MICP-treated sands. A few samples, however, such as SLS-3-40 and SLS-4-400, exhibited a larger C_α relative to the sustained stress level, exceeding the expected range suggested by the ILS data. For such cases, the time factor was also key in determining the contribution of secondary compressibility to the overall response.

To better isolate the evolution of delayed deformation with elapsed time, Fig. 9 presents the axial strains normalized to the initial value recorded after immediate loading. Five treated samples, at both 40 and 400 kPa, showed continuous strain accumulation following initial deformation at a decreasing rate that eventually stabilized to form a plateau, beyond which there was no major strain accumulation, also referred to as fading creep (Mitchell and Solymar 1987). The same behavior was exhibited by the control natural sand sample (SLS-0-400). In contrast, four marked samples in Fig. 9 reveal a yield point at which the stabilization process was instead reversed to accelerate strain rate accumulation before stagnating again. For these samples, a sustained load over time triggered delayed destructuration in the form of punctual events similar to stress increase events, albeit of a lower magnitude.

Time-Dependent Characteristics

To compare the behavior of all tests, it is possible to normalize the preconsolidation pressure of a test (p_c') to the effective vertical stress (σ_v') at each loading step. For all samples, for both the medium and fine sands, the variation in C_α rapidly increased when σ_v' exceeded the recorded p_c' for each test, as shown in Fig. 10. Additionally, when examining the loading curves for all the steps of the conducted tests, such as the example shown in Fig. 6, the deformation of biocemented sands appeared to repeatably stabilize under the sustained load before eventually yielding with an additional deformation increment. Such a progressive deformation that mobilized in stages highlights an overstressed matrix typical of perceived apparent ductility conveyed to a system by crushable components, continuously shifting the inner fabric to a temporary

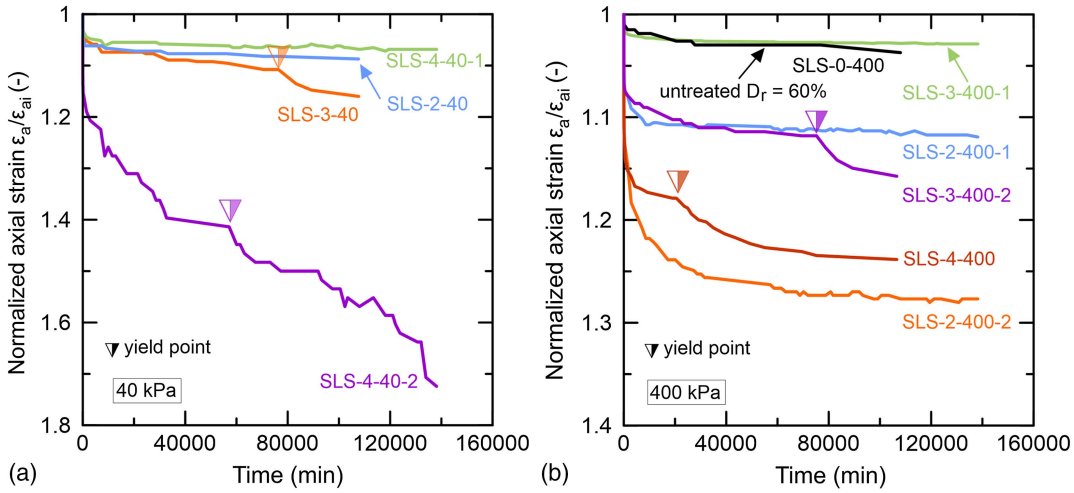

Fig. 9. Normalized axial strain for a sustained effective vertical stress of (a) 40 kPa; and (b) 400 kPa.

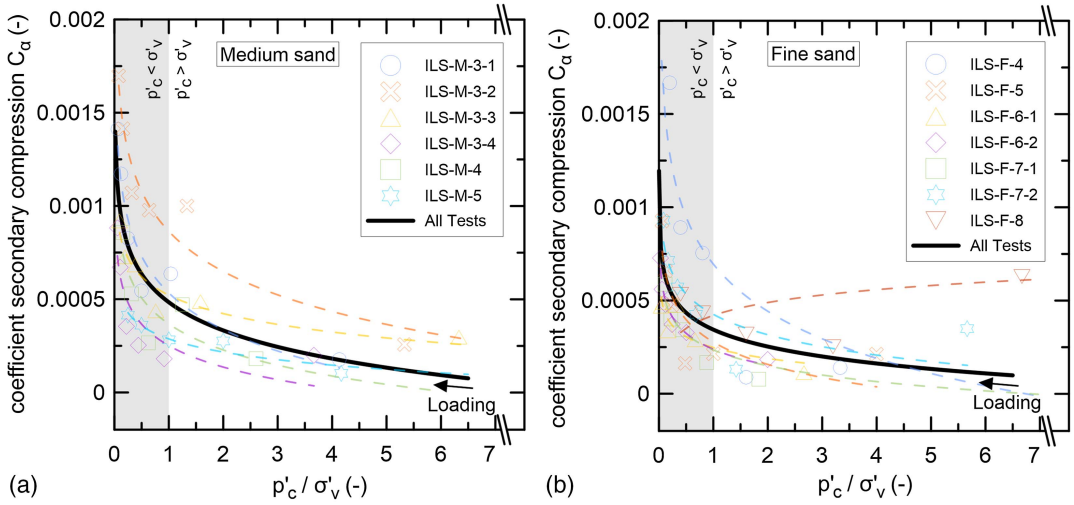

Fig. 10. Variation in the coefficient of secondary compression with the normalized pressure ratio per loading step for (a) medium-grained; and (b) fine-grained sands.

equilibrium before breaking with each deformation increment (Ciantia et al. 2017). This dependence between the theoretical onset of damage in a sample (p_c') and an accelerating creep response highlights the interdependence between stress- and time-related phenomena, as the latter could not be dissociated from structural damage in the fabric, itself conveyed to a sample by MICP treatment. A study of the damage to artificially cemented soils using mercury intrusion porosimetry found slow damage evolution in the quasi-elastic stage, which then evolved more rapidly with increasing stress (Huie et al. 2018). Such concepts have been proposed in recent studies, where, for instance, the initiation of bond breakage has been attributed to the bilinear feature of the void ratio versus the logarithm of vertical stress plots, marking the transition between different stages of the compression response (Xiao et al. 2020).

Discussion

The stress-strain-time relations of soils are often regarded as a sum of two structural deformation mechanisms: sliding deformation, or particle rearrangement, and cataclastic deformation, or particle crushing (Feda 1992). An experimental study based on natural sand under similar oedometric compression captured sliding at intergranular contacts as the principal mechanism of creep in granular material (Andò et al. 2019). In contrast, the matrix of structured soil is locked as the direct effect of the cementing agent. Figs. 11(a and b) shows the different deposition patterns of $CaCO_3$ due to MICP treatment, as observed from SEM. Aside from grain coating, also referred to as passive coating due to its purely densifying role and lack of contribution to direct load transfer, $CaCO_3$ can precipitate at existing contact points between grains or bridge a new matrix-supporting bond. Only the latter two constitute the active bonds of a biocemented soil. Rearrangement can thus also take place in a treated soil but only after active bonds are broken. If particle crushing in a pure quartz lattice under 1,000 kPa remains unlikely (Andò et al. 2019; Xiao et al. 2020), the quartz-carbonate matrix of a biocemented sand allows for more cataclastic deformation to contribute to the overall response, as the properties of its constituents can be inherently different, for instance in shear and bulk moduli, as mentioned in a previous section. Indeed, $CaCO_3$ breakage is possible on weak planes or edges, especially for precipitation cases in biogenic conditions, where $CaCO_3$ can assume different phases, forms, and sizes (Clarà Saracho et al. 2020), along with retaining multiple flaws due to the treatment, such as bacterial traces or deposition fronts, as captured in Figs. 11(c and d). Such fabric defects were at the root of the delayed yield events recorded for some samples in the sustained loading series, as the behavior did not strictly align with the treatment level or applied stress. The same was noted in a study based on mineralogical calcite, where the cracked profiles did not appear to be ruled by the applied stress but most likely depended on the presence or absence of a flaw in the calcite (Croizé et al. 2010).

A potential for rearrangement of grains can be defined as a property of the initial state of soil, with, most notably, soil type, granulometry, and initial density. With MICP, a treated soil retains its initial configuration, only to be altered by the addition of $CaCO_3$ to its composition in the form of passive or active bonds. With its initial matrix mostly unchanged, the soil lattice retains the same potential for rearrangement but is locked after treatment is concluded. For natural sand, most sliding takes place immediately after loading, thus dissipating the potential for rearrangement relative to the stress level, resulting in little to no further change with time. For biocemented sand, however, loading results only in partial dissipation of this potential as immediate deformation, causing a sliding tendency in the soil, which can be later released if the active bonds are damaged. This degradation of active bonds took place for different loading configurations, such as (1) increasing stresses, (2) sustained loading, or even (3) unloading-reloading to a stress level exceeding p_c' (observed at 500 kPa). The treatment thus shifts a portion of the quasi-instantaneous compressibility, typical of granular material due to rearrangement, to be released as "delayed" sliding when the matrix yields to the sustained applied stress because of a collapse of flawed or fatigued bonds after being continuously overstressed. A schematic of the different behaviors is shown in Fig. 12, differentiating between the two observed regimes relative to the state of a treated sample based on its loading history (intact or damaged), with p_c' as the threshold for major onset of damage, as suggested by Huie et al. (2018) and Xiao et al. (2020). In this case, the origin of creep in MICP-treated sands was not the ductility or viscous flow of the precipitated $CaCO_3$ crystals but rather their breakage due to overstress in the fabric, as was observed throughout the experiments. Hence, the creep response and the stress level

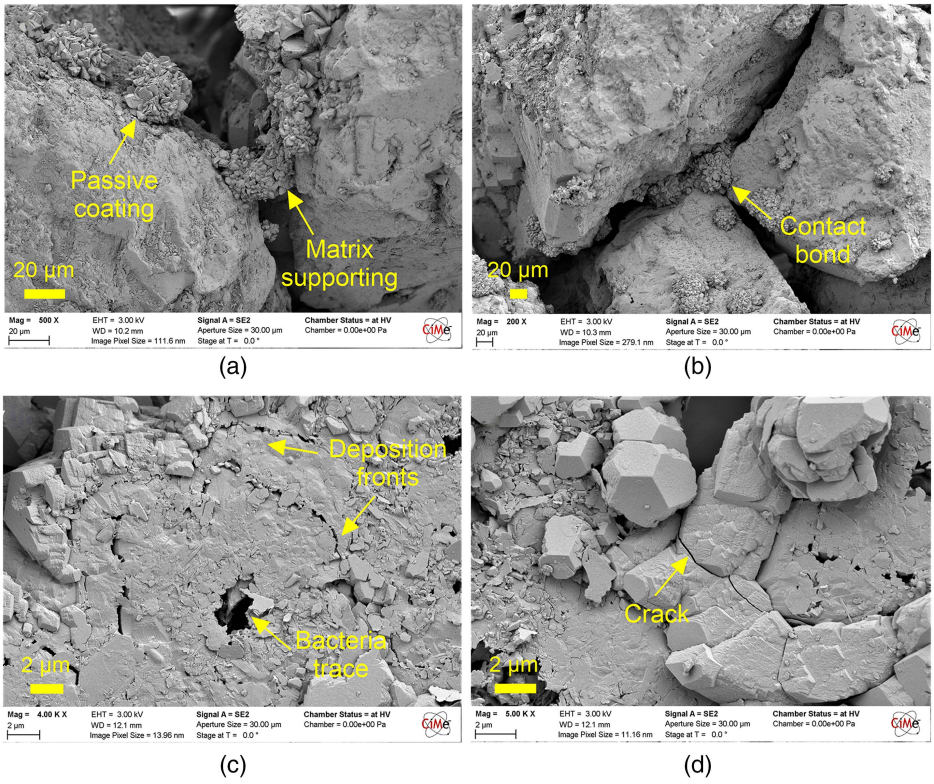

Fig. 11. SEM images: (a) passive coating and matrix-supporting bond in the void between two grains; (b) cementation at the contact point; (c) bacteria trace and deposition fronts with successive injections captured at the interface with a detached grain; and (d) crack through precipitated calcium carbonate.

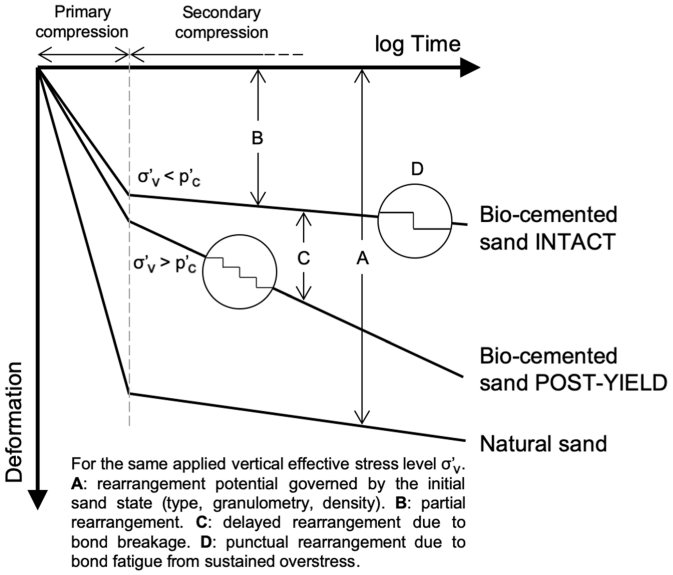

Fig. 12. Schematic trends summary of natural and biocemented sand behaviors.

and its effect on the matrix should not be dissociated since it is essentially governed by debonding.

Models of the time-dependent behavior of soils that exist in the literature are categorized into three large families: empirical, rheological, and general stress-strain-time (Liingaard et al. 2004). Overall, most existing time-related models were theoretically developed for clays, rendering their use generally unsuitable for the time-dependent behavior of sand (Liingaard et al. 2004). Moreover, models that interpret the reduction in void ratio during creep as leading to an improved inner structure are fundamentally inadequate for biocemented sands, as captured in this study.

Conclusions

In the work presented here, the stress- and time-dependent compressibilities of two biocemented sands with different densities and treatment levels were investigated. The preliminary deformation characteristics and patterns captured in the experimental plan were discussed with respect to various existing frameworks to characterize the underlying mechanisms behind the deformation of bonded materials. The major findings are summarized as follows:

- MICP significantly reduced the compressibility of medium and fine sands, more so at higher treatment levels. The recorded axial strains for most samples were notably lower than those for the equivalent untreated state, and oedometric moduli values even reached 450 and 700 MPa, bordering the domain of sandstones.
- The observed enhancement achieved by the treatment was not absolute but stress-dependent, as successive loading steps were accompanied by a degradation front that progressively negated the role of active bonds in the soil lattice. This debonding was observed to take place gradually without immediate collapse.
- Treated sands remained soil-like, as their response to accumulated damage eventually diverged based on their respective initial conditions (sand type, granulometry, and compacity), which

should be considered along with the expected loading stress when deciding on a treatment level for an envisaged intervention.
- For medium sand, the η/C_{iv} ratio initially developed for artificially cemented soils could also be applied for biocemented cases. A more efficient cementation with a wider range of η/C_{iv} values could be more successful in applying this ratio to fine MICP-treated sands.
- Sustained loading resulted in delayed debonding events. More generally, under higher stresses secondary compressibility contributed a higher proportion to total settlement, where C_α was found to be up to three times larger than that in the equivalent natural state.
- Creep response could not be dissociated from stress considerations. In this case, the origin of creep in MICP-treated sands was not ductility or viscous flow of the precipitated $CaCO_3$ crystals but rather their progressive breakage.
- MICP treatment caused a shift in the immediate settlement observed in the natural state to be released as creep after delayed rearrangement of grains took place due to bond breakage, which was caused by (1) increasing stresses, (2) sustained loading, or (3) unloading-reloading.

Data Availability Statement

Some or all data, models, or code that support the findings of this study are available from the corresponding author upon reasonable request.

Acknowledgments

The authors would like to acknowledge the financial support of the European Research Council (ERC) under the European Union's Horizon 2020 research and innovation program (Grant No. 788587).

Notation

The following symbols are used in this paper:

C (%) = gravimetric calcium carbonate content;
C_c = compression index;
C_{iv} (%) = volumetric calcium carbonate content;
C_r = recompression index;
C_α = coefficient of secondary compression;
D_r (%) = relative density;
D_{10} (μm) = 10% passing diameter;
D_{50} (μm) = 50% passing diameter;
E_{oed} (MPa) = oedometric modulus;
e_i = void ratio before treatment;
e_0 = void ratio after treatment;
m_c (g) = calcium carbonate mass;
m_d (g) = total dry sample mass;
p'_c (kPa) = preconsolidation stress;
V_c (mm^3) = volume of calcium carbonate;
ε_a (%) = axial strain;
ε_{ai} (%) = axial strain after immediate loading;
ρ_c (g/cm^3) = calcium carbonate density;
σ'_v (kPa) = effective vertical stress; and
η/C_{iv} = porosity-to-cement ratio.

References

Andò, E., J. Dijkstra, E. Roubin, C. Dano, and E. Boller. 2019. "A peek into the origin of creep in sand." *Granular Matter* 21 (1): 1–8. https://doi.org/10.1007/s10035-018-0863-5.

ASTM. 2007. *Standard test method for particle-size analysis of soils*. ASTM D422-63. West Conshohocken, PA: ASTM.

ASTM. 2018. *Standard practice for classification of soils for engineering purposes (unified soil classification system)*. ASTM D2487-17. West Conshohocken, PA: ASTM.

ASTM. 2020. *One-dimensional consolidation properties of soils using incremental loading*. ASTM D2435/D2435M-11. West Conshohocken, PA: ASTM.

Belkofsi, R., O. Adjaoud, and I. Belabbas. 2018. "Pressure induced phase transitions and elastic properties of CaCO3 polymorphs: A density functional theory study." *Modell. Simul. Mater. Sci. Eng.* 26 (6): 065004. https://doi.org/10.1088/1361-651X/aacbed.

Ciantia, M. O., G. Piñero, J. Zhu, and T. Shire. 2017. "On the progressive nature of grain crushing." In Vol. 140 of *Proc., EPJ Web of Conf.*, 07006. Les Ulis, France: EDP Sciences.

Clarà Saracho, A., S. K. Haigh, T. Hata, K. Soga, S. Farsang, S. A. T. Redfern, and E. Marek. 2020. "Characterisation of CaCO3 phases during strain-specific ureolytic precipitation." *Sci. Rep.* 10 (1): 1–12. https://doi.org/10.1038/s41598-020-66831-y.

Consoli, N. C., A. V. da Fonseca, S. R. Silva, R. C. Cruz, and A. Fonini. 2012. "Parameters controlling stiffness and strength of artificially cemented soils." *Géotechnique* 62 (2): 177–183. https://doi.org/10.1680/geot.8.P.084.

Consoli, N. C., A. Fonini, S. Maghous, F. Schnaid, and A. Viana Da Fonseca. 2013. "Experimental analysis of the mechanical properties of artificially cemented soils and their evolution in time." In Vol. 1 of *Proc., 18th Int. Conf. on Soil Mechanics and Geotechnical Engineering: Challenges and Innovations in Geotechnics, ICSMGE 2013*, 321–324. Paris: Presses des Ponts.

Consoli, N. C., D. Foppa, L. Festugato, and K. S. Heineck. 2007. "Key parameters for strength control of artificially cemented soils." *J. Geotech. Geoenviron. Eng.* 133 (2): 197–205. https://doi.org/10.1061/(ASCE)1090-0241(2007)133:2(197).

Consoli, N. C., E. J. B. Marin, R. A. Q. Samaniego, H. C. S. Filho, and N. M. C. Cristelo. 2019. "Field and laboratory behaviour of fine-grained soil stabilised with lime." *Can. Geotech. J.* 57 (6): 933–938. https://doi.org/10.1139/cgj-2019-0271.

Croizé, D., F. Renard, K. Bjørlykke, and D. K. Dysthe. 2010. "Experimental calcite dissolution under stress: Evolution of grain contact microstructure during pressure solution creep." *J. Geophys. Res.* 115 (B9). https://doi.org/10.1029/2010jb000869.

De Yoreo, J. J., et al. 2015. "Crystallization by particle attachment in synthetic, biogenic, and geologic environments." *Science* 349 (6247): 6760.1–6760.8. https://doi.org/10.1126/science.aaa6760.

Diambra, A., E. Ibraim, L. Festugato, and M. B. Corte. 2021. "Stiffness of artificially cemented sands: Insight on characterisation through empirical power relationships." *Road Mater. Pavement Des.* 22 (6): 1469–1479. https://doi.org/10.1080/14680629.2019.1705379.

Di Prisco, C., and S. Imposimato. 1996. "Time dependent mechanical behaviour of loose sands." *Mech. Cohesive-Frict. Mater.* 1 (1): 45–73. https://doi.org/10.1002/(SICI)1099-1484(199601)1:1<45::AID-CFM3>3.0.CO;2-O.

Esnault-Filet, A., J.-P. Gadret, L. Memphis, and S. Borel. 2012. "Biocalcis and its applications for the consolidation of sands." In *Proc., 4th Int. Conf. on Grouting and Deep Mixing*, 1767–1780. Reston, VA: ASCE. https://doi.org/10.1061/9780784412350.

Feda, J. 1992. *Creep of soils and related phenomena.* Amsterdam: Elsevier.

Feng, K., and B. M. Montoya. 2014. "Behavior of bio-mediated soil in k0 loading." In *Proc., Geo-Shanghai 2014*, 1–10. Reston, VA: ASCE. https://doi.org/10.1061/9780784413456.001.

Feng, K., and B. M. Montoya. 2016. "Influence of confinement and cementation level on the behavior of microbial-induced calcite precipitated sands under monotonic drained loading." *J. Geotech. Geoenviron. Eng.* 142 (1): 1–9. https://doi.org/10.1061/(ASCE)GT.1943-5606.0001379.

Huie, C., C. Zongfang, Z. Chuanfeng, Z. Jun, and Y. Xiaoqing. 2018. "Damage evolution process of cement-stabilized soil based on deformation and microstructure analysis." *Mar. Georesour. Geotechnol.* 36 (1): 64–71. https://doi.org/10.1080/1064119X.2017.1279246.

Länsivaara, T. T. 2020. "Determination of creep properties of clays from VRS oedometer tests." *Geotech. Geol. Eng.* 38 (2): 1857–1871. https://doi.org/10.1007/s10706-019-01135-1.

Lashin, I., M. Ghali, M. N. Hussien, M. Chekired, and M. Karray. 2021. "Investigation of small- to large-strain moduli correlations of normally consolidated granular soils." *Can. Geotech. J.* 58 (1): 1–22. https://doi.org/10.1139/cgj-2019-0741.

Lee, M. L., W. S. Ng, and Y. Tanaka. 2013. "Stress-deformation and compressibility responses of bio-mediated residual soils." *Ecol. Eng.* 60 (Nov): 142–149. https://doi.org/10.1016/j.ecoleng.2013.07.034.

Liingaard, M., A. Augustesen, and P. V. Lade. 2004. "Characterization of models for time-dependent behavior of soils." *Int. J. Geomech.* 4 (3): 157–177. https://doi.org/10.1061/(ASCE)1532-3641(2004)4:3(157).

Lin, H., M. T. Suleiman, D. G. Brown, and E. Kavazanjian. 2016. "Mechanical behavior of sands treated by microbially induced carbonate precipitation." *J. Geotech. Geoenviron. Eng.* 142 (2): 1–13. https://doi.org/10.1061/(ASCE)GT.1943-5606.0001383.

Mendoza-Ulloa, J. A., D. Lombardi, and S. M. Ahmad. 2020. "Small-strain stiffness degradation of artificially cemented sands." *Géotech. Lett.* 10 (2): 1–19. https://doi.org/10.1680/jgele.19.00021.

Mesri, G., and B. Vardhanabhuti. 2009. "Compression of granular materials." *Can. Geotech. J.* 46 (4): 369–392. https://doi.org/10.1139/T08-123.

Mitchell, J. K., and Z. V. Solymar. 1987. "Time-dependent strength gain in freshly deposited or densified sand." *J. Geotech. Eng.* 113 (2): 176. https://doi.org/10.1061/(ASCE)0733-9410(1987)113:2(176).

Montoya, B. M., S. Safavizadeh, and M. A. Gabr. 2019. "Enhancement of coal ash compressibility parameters using microbial-induced carbonate precipitation." *J. Geotech. Geoenviron. Eng.* 145 (5): 04019018. https://doi.org/10.1061/(ASCE)GT.1943-5606.0002036.

Nafisi, A., and B. M. Montoya. 2018. "A new framework for identifying cementation level of MICP-treated sands." In *IFCEE 2018: Innovations in Ground Improvement for Soils, Pavements, and Subgrades*, Geotechnical Special Publication 296, edited by A. W. Stuedlein, A. Lemnitzer, and M. T. Suleiman, 37–47. Reston, VA: ASCE. https://doi.org/10.1061/9780784481592.005.

Schmitt, D. R. 2015. *Geophysical properties of the near surface earth: Seismic properties*. Amsterdam: Elsevier.

Tang, C. S., L. Yin, J. Yang, N. Jun, C. Zhu, H. Zeng, H. Li, and B. Shi. 2020. "Factors affecting the performance of microbial-induced carbonate precipitation (MICP) treated soil: A review." *Environ. Earth Sci.* 79 (5): 1–23. https://doi.org/10.1007/s12665-020-8840-9.

Terzis, D., and L. Laloui. 2018. "3-D micro-architecture and mechanical response of soil cemented via microbial-induced calcite precipitation." *Sci. Rep.* 8 (1): 1–11. https://doi.org/10.1038/s41598-018-19895-w.

Terzis, D., and L. Laloui. 2019a. "A decade of progress and turning points in the understanding of bio-improved soils: A review." *Geomech. Energy Environ.* 19 (Sep): 100116. https://doi.org/10.1016/j.gete.2019.03.001.

Terzis, D., and L. Laloui. 2019b. "Cell-free soil bio-cementation with strength, dilatancy and fabric characterization." *Acta Geotech.* 14 (3): 639–656. https://doi.org/10.1007/s11440-019-00764-3.

Wang, J., Z. Mao, F. Jiang, and T. S. Duffy. 2015. "Elasticity of single-crystal quartz to 10 GPa." *Phys. Chem. Miner.* 42 (3): 203–212. https://doi.org/10.1007/s00269-014-0711-z.

Wichtmann, T., I. Kimmig, and T. Triantafyllidis. 2017. "On correlations between 'dynamic' (small-strain) and 'static' (large-strain) stiffness moduli—An experimental investigation on 19 sands and gravels." *Soil Dyn. Earthquake Eng.* 98 (Apr): 72–83. https://doi.org/10.1016/j.soildyn.2017.03.032.

Xiao, Y., C. Zhao, Y. Sun, S. Wang, H. Wu, H. Chen, and H. Liu. 2020. "Compression behavior of MICP-treated sand with various gradations." *Acta Geotech.* 16 (5): 1391–1400. https://doi.org/10.1007/s11440-020-01116-2.

Yuan, J., D. Lei, Y. Shan, H. Tong, X. Fang, and J. Zhao. 2022. "Direct shear creep characteristics of sand treated with microbial-induced calcite precipitation." *Int. J. Civ. Eng.* 8 (Jan): 1–5. https://doi.org/10.1007/s40999-021-00696-8.

Yun, T. S., and J. C. Santamarina. 2005. "Decementation, softening, and collapse: Changes in small-strain shear stiffness in k_0 loading." *J. Geotech. Geoenviron. Eng.* 131 (3): 350–358. https://doi.org/10.1061/(ASCE)1090-0241(2005)131:3(350).